Tribol Lett (2008) 29:95–103
DOI 10.1007/s11249-007-9286-x

ORIGINAL PAPER

Adaptive $Mo_2N/MoS_2/Ag$ Tribological Nanocomposite Coatings for Aerospace Applications

Samir M. Aouadi · Yadab Paudel · Brandon Luster · Shane Stadler · Punit Kohli · Christopher Muratore · Carl Hager · Andrey A. Voevodin

Received: 24 September 2007 / Accepted: 29 November 2007 / Published online: 20 December 2007

Abstract Reactively sputtered $Mo_2N/MoS_2/Ag$ nanocomposite coatings were deposited from three individual Mo, MoS_2, and Ag targets in a nitrogen environment onto Si (111), 440C grade stainless steel, and inconel 600 substrates. The power to the Mo target was kept constant, while power to the MoS_2 and Ag targets was varied to obtain different coating compositions. The coatings consisted of Mo_2N, with silver and/or sulfur additions of up to approximately 24 at%. Coating chemistry and crystal structure were evaluated using X-ray photoelectron spectroscopy (XPS) and X-ray diffraction (XRD), which showed the presence of tetragonal Mo_2N and cubic Ag phases. The MoS_2 phase was detected from XPS analysis and was likely present as an amorphous inclusion based on the absence of characteristic XRD peaks. The tribological properties of the coatings were investigated in dry sliding at room temperature against Si_3N_4, 440C stainless steel, and Al_2O_3. Tribological testing was also conducted at 350 and 600 °C against Si_3N_4. The coatings and respective wear tracks were examined using scanning electron microscopy (SEM), optical microscopy, profilometry, energy dispersive X-ray spectroscopy (EDX), and micro-Raman spectroscopy. During room temperature tests, the coefficients of friction (CoF) were relatively high (0.5–1.0) for all coating compositions, and particularly high against Si_3N_4 counterfaces. During high-temperature tests, the CoF of single-phase Mo_2N coatings remained high, but much lower CoFs were observed for composite coatings with both Ag and S additions. CoF values were maintained as low as 0.1 over 10,000 cycles for samples with Ag content in excess of 16 at% and with sulfur content in the 5–14 at% range. The chemistry and phase analysis of coating contact surfaces showed temperature-adaptive behavior with the formation of metallic silver at 350 °C and silver molybdate compounds at 600 °C tests. These adaptive $Mo_2N/MoS_2/Ag$ coatings exhibited wear rates that were two orders of magnitude lower compared to Mo_2N and Mo_2N/Ag coatings, hence providing a high potential for lubrication and wear prevention of high-temperature sliding contacts.

Keywords Self-lubricating friction · Solid lubricants · Raman · Solid lubricated wear · Coatings · Friction-reducing

S. M. Aouadi (✉) · Y. Paudel · B. Luster · S. Stadler
Department of Physics, Southern Illinois University, Carbondale, IL 62901, USA
e-mail: saouadi@physics.siu.edu

P. Kohli
Department of Chemistry, Southern Illinois University, Carbondale, IL 62901, USA

C. Muratore · C. Hager · A. A. Voevodin
Air Force Research Laboratory, Materials and Manufacturing Directorate, Wright-Patterson Air Force Base, Dayton, OH 45433, USA

1 Introduction

In the last decade, thin layers of molybdenum nitride (Mo–N) have been investigated as materials with a wide variety of potential applications that include catalysis [1, 2], superconductivity [3, 4], diffusion barriers for copper interconnects [5], gate electrode materials for high-*k* gate dielectrics [6, 7], and as corrosion- and wear-resistant coatings [8, 9]. The Mo–N system was reported to crystallize in three possible phases, namely, face-centered cubic Mo_2N, tetragonal Mo_2N, and hexagonal MoN [8].

Unlike other transition metal nitrides, such as TiN and CrN, which have been investigated for a few decades now, interest in Mo–N as a potential material for tribological

applications is very recent. The impetus for investigating this material stems from its superior mechanical properties (hardness reported to be in the 28–34 GPa range compared to 18–24 GPa for TiN and CrN) and the lubricating properties of its surface oxides (MO_x) at elevated temperatures (>300 °C) which is due to the presence of lamellar structures (Magnéli phases) that shear easily during contact loading [10–13].

Recently, additional alloying elements were incorporated into the design of Mo–N based materials to produce nanocomposite coatings [14]. These materials usually exhibit superior mechanical and tribological properties compared to their constituent phases [14, 15]. Two groups of hard nanocomposite structures are known to provide such enhanced mechanical and tribological properties [16]: (1) coatings containing two hard phases such as nc-TMN/a-Si_3N_4 (TM = transition metals such as Ti, Cr, Nb, etc.; nc- and a- denote the nanocrystalline and amorphous phases, respectively) or nc-TiN/a-BN, and (2) materials containing a hard phase and a soft phase such as nc-TMN/Me (Me = soft metals such as Cu, Ag, Co, etc.). Some of the advantages of the former group include the possibility to reach hardness values in excess of 40 GPa (ultra-hard coatings) and thermal stability at temperatures up to 1,100 °C (properties that would be valuable for cutting tools, for example). The benefit of using the latter group of materials is the improved fracture toughness and the self-lubricating potential, provided by the soft metal, at high temperature (properties that are important for rolling element bearings, air foil bearings, gears, etc.) In the literature, alloying elements that were incorporated in the MO–N coatings include Cu [17, 18], Ag [19, 20], Si [21, 22], and C [23]. The addition of the optimum amount of these alloying elements was found to provide enhanced mechanical (toughness) and tribological (reduced friction coefficient and wear rate) properties. This is explained further in this article for a complex 3-phase material system made of Mo_2N, MoS_2, and Ag.

The aim of the current article is to provide a comprehensive study of the mechanical and frictional properties of Mo_2N/MoS_2/Ag self-lubricating coatings for high-temperature tribological applications. It is intended that these coatings will provide a "chameleon" surface adaptation that adjusts its surface composition and structure to minimize friction as the working environment changes [13, 24–26]. The Mo_2N phase offers good mechanical and lubricating properties at high temperature, as indicated earlier in this section. The addition of both MoS_2 and Ag can reduce friction at moderately high temperatures (300–400 °C) since both ingredients are lubricious under these conditions. At higher temperatures, however, the formation of silver molybdate compounds [19, 24], such as Ag_2MoO_4, $Ag_2Mo_2O_7$, and $Ag_2Mo_4O_{13}$, facilitated by the presence of MoS_2 [24], is expected to be an effective mechanism for friction reduction. These molybdate compounds were predicted to be lubricious by the crystal chemical model [27], which was used to account for the formation of low shear/friction tribofilms in sliding contacts.

The tribological properties of Mo_2N/MoS_2/Ag self-lubricating coatings deposited by unbalanced magnetron sputtering were evaluated at room temperature (RT), at 350, and at 600 °C. Emphasis is placed on the high-temperature tribological properties, since these materials were designed to be self-lubricating under these conditions. Also, most of the tribotesting was carried out using Si_3N_4 as a counterpart material in dry sliding conditions since it is stable throughout the desired test temperature range practically used in hybrid bearings of jet engines and other high temperature and space applications. It is important to note that the friction coefficient values of nitride on nitride surfaces reported in the literature were very high (friction coefficients in excess of 0.8 at RT) [28, 29]. The CoF of nitride-based coatings at high temperature are also high (usually >0.5) [30] even against other counterfaces such as stainless steel or alumina [31]. It was expected that the addition of the selected lubricious phases would significantly improve the tribological properties of these coatings.

2 Experimental Procedure

Mo_2N/MoS_2/Ag thin coatings were deposited on hardened 440C grade stainless steel and on inconel 600 substrates using an unbalanced magnetron sputtering apparatus that was described in detail elsewhere [32]. The substrates were cleaned ultrasonically in acetone and methanol for 15 min and successively rinsed with deionized water and blown with dry N_2. The coatings were grown using individual targets of Mo, MoS_2, and Ag that were 5 cm in diameter. The base pressure of the system was lower than 1×10^{-5} Pa prior to each coating deposition. The coatings were grown in a mixed atmosphere of Ar (99.999% purity) and N_2 (99.99% purity) with partial pressures that were set to 0.3 and 0.04 Pa, respectively. During deposition, the power to the Mo target was fixed at 200 W and the power to the MoS_2 and Ag sources were varied, as shown in Table 1. Table 1 provides the coating nomenclature designation, which is used throughout the text and figures. The substrates were held at a bias voltage of −60 V and were continuously rotated about their polar axis with a rotational speed of 50 rpm. The coatings were grown for 1.5 h at a substrate temperature of 350 °C leading to coating thicknesses in the 2.8 ± 0.3 μm range.

Structural characterization of the deposited coatings was carried out using a GBS MMA (Mini materials analyzer) X-ray diffractometer. All spectra were taken using Cu-Kα

Table 1 Nomenclature, deposition conditions, and composition of $Mo_2N/MoS_2/Ag$ coatings obtained by magnetron sputtering of Mo, Ag, and MoS_2 targets. The first number in the coating nomenclature corresponds to the power to the Ag target whereas the second number corresponds to the power to the MoS_2 target. Both powers were the variable deposition parameters in this study

Coating	S-0-0	S-50-40	S-30-20	S-27-0	S-14-40	S-20-20
P_{Ag} (W)	0	50	30	27	14	20
P_{MoS2} (W)	0	40	20	0	40	20
Mo (at%)	63	40	45	48	47	47
N (at%)	37	27	34	36	32	35
S (at%)	0	9	5	0	13	6
Ag (at%)	0	24	16	16	8	12

radiation with an accelerating voltage of 35 kV and a current of 30 mA. The elemental and phase compositions were determined using a Leybold Max 200 X-ray photoelectron spectroscopy (XPS) analyzer and a Renishaw SPM micro-Raman system. Scanning electron microscopy (SEM) was performed using a Hitachi S570, operating at 20 kV, to analyze the morphology of the coatings before and after wear testing. The SEM system was equipped with an energy dispersive X-ray (EDX) apparatus for elemental analysis.

A Nanovea ball on disk tribotester (Microphotonics, Irvine, CA) was employed for the evaluation of wear and friction behavior at room temperature under two conditions: (1) in air (50 ± 5% relative humidity) and (2) in dry nitrogen. Three different counterpart materials were used during tribotesting: (1) alumina, (2) 440C stainless steel (SS), and (3) Si_3N_4 balls with a diameter of 6 mm. The measurements were carried out using a normal load of 1 N and a sliding rate of 0.2 m/s for 10,000 cycles. A high-temperature tribotester was subsequently used to test the performance of the deposited coupons at 350 and 600 °C using Si_3N_4 balls as counterparts with the same conditions as those used for room temperature testing. Wear rates were then determined from the cross section of the wear track, measured using multiple profilometry line scans of the surface. Counterpart wear was investigated qualitatively with microscopy and also by identification of counterpart species via surface analysis in coating wear tracks.

3 Results and Discussion

3.1 As Deposited Coatings

The X-ray diffraction pattern of MO–N coatings, shown in Fig. 1, is characteristic of tetragonal β-Mo_2N (JCPDS card no.: 75-1,150) [33]. Grain size was estimated from the

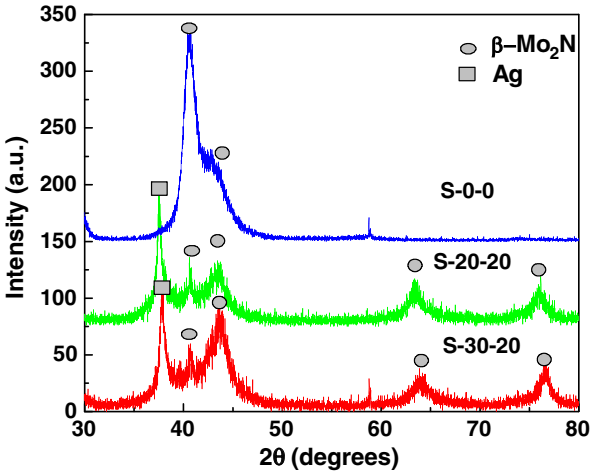

Fig. 1 XRD data for selected as deposited coatings

Scherrer formula to be about 15 nm [32]. The addition of Ag and MoS_2 resulted in a broadening in the β-Mo_2N diffraction peaks (due to the grain refinement that originated from the creation of a nanocomposite structure [32, 34] and the appearance of new ones that correspond to face centered cubic silver, as shown in Fig. 1.

The atomic concentrations of Mo, Ag, S, and N were quantified with the XPS technique and are summarized in Table 1. The Mo_{3d}, Ag_{3d}, S_{2p}, and N_{1s} peaks were located at 228.2, 368.5, 162.4, and 397.2 eV, respectively. A conventional curve-fitting method was utilized to determine the contribution from the N_{1s} peak since it overlapped with the tail of the Mo_{3p} peak [35]. The binding energy of the $Mo_{3d5/2}$ peak was similar to the one reported for the lower valence state Mo^{2+} that corresponds to molybdenum nitride (228.4 ± 0.2 eV) [35]. The position of the N_{1s} peak was in agreement with the values reported for Mo_2N (397.4 ± 0.2 eV) [35]. The S_{2p} line consists of a singlet peak with a binding energy value that corresponds to S^{2-} [36]. This indicates that the sulfur species were bonded to Mo atoms in an MoS_2 phase which was, however, amorphous as suggested by the absence of characteristic hexagonal MoS_2 peaks in XRD spectra. Finally, the binding energy of the Ag_{3d} peak is typical of a metallic Ag–Ag bond (368.7 ± 0.2 eV) [32].

3.2 Room Temperature Tests

The average coefficients of friction (CoF) measured during tribological tests with the different counterpart materials in both air and dry nitrogen environments are presented in Table 2. In air, the CoF for Mo_2N was found to be the highest when tested against Si_3N_4 ($\mu = 1.06$) and the lowest when tested against Al_2O_3 ($\mu = 0.28$). In dry nitrogen, however, the CoF was found to be the highest

Table 2 Coefficients of friction and wear rates for $Mo_2N/MoS_2/Ag$ coatings obtained in sliding tests against Al_2O_3, Si_3N_4, and stainless steel (SS) balls tested at room temperature in air and in dry nitrogen, at 350 °C in air, and at 600 °C in air

Coating	S-0-0	S-50-40	S-30-20	S-27-0	S-14-40	S-20-20
Coefficients of friction at room temperature						
Al_2O_3/Air	0.28	0.52	0.54	0.69	0.56	0.67
Al_2O_3/N_2	0.85	0.49	0.60	0.68	0.59	0.72
Si_3N_3/Air	1.06	0.62	0.42	0.55	0.80	0.70
Si_2N_3/N_2	0.67	0.80	0.52	0.60	0.76	0.73
SS/Air	0.42	0.68	0.54	0.62	0.74	0.72
SS/N_2	0.27	0.70	0.45	0.57	0.69	0.66
Wear rates in mm^3/(nm) at room temperature						
Al_2O_3/Air	Little wear	3×10^{4}	2×10^{-4}	4×10^{-4}	9×10^{-5}	9×10^{-5}
Al_2O_3/N_2	9×10^{-5}	5×10^{-4}	3×10^{-4}	6×10^{-4}	1×10^{-4}	2×10^{-4}
Si_3N_3/Air	Little wear	6×10^{-4}	3×10^{-4}	7×10^{-4}	1×10^{-4}	6×10^{-5}
Si_2N_3/N_2	5×10^{-5}	4×10^{-4}	4×10^{-4}	8×10^{-4}	2×10^{-4}	1×10^{-4}
SS/Air	3×10^{-6}	5×10^{-4}	4×10^{-4}	7×10^{-4}	9×10^{-5}	3×10^{-4}
SS/N_2	Little wear	3×10^{-4}	3×10^{-4}	5×10^{-4}	8×10^{-5}	2×10^{-4}
Coefficients of friction and wear rates in mm^3/(nm) against Si_3N_4 at 350 °C air						
CoF	0.80	0.37	0.37	0.40	0.45	0.40
Wear rate	7×10^{-5}	9×10^{-5}	7×10^{-5}	6×10^{-5}	5×10^{-5}	4×10^{-5}
Coefficients of friction and wear rates in mm^3/(nm) against Si_3N_4 at 600 °C air						
CoF	0.72	0.10	0.10	0.45	0.18	0.23
Wear rate	5×10^{-4}	8×10^{-6}	1×10^{-5}	1×10^{-4}	6×10^{-5}	4×10^{-5}

against Al_2O_3 ($\mu = 0.85$), and the lowest against SS ($\mu = 0.27$). The addition of MoS_2 and Ag was found to improve the frictional properties against Si_3N_4. For example, the measured CoF for coating S-30-20 was 0.42 and 0.52 in air and dry nitrogen, respectively. SEM images of the wear tracks for this particular coating sample are shown in Fig. 2. The wear in contact with Al_2O_3 was less than with SS or Si_3N_4. However, the counterpart wear of Al_2O_3 was greater than that of SS or Si_3N_4. The wear tracks were analyzed using Raman spectroscopy. All spectra displayed a broad peak centered at 903 cm^{-1} which belongs to the monoclinic β-MoO_3 phase [37]. EDX data displayed in Fig. 2 revealed that some of the coating was worn through (dark regions) when tested in air against Al_2O_3 and Si_3N_4. This was probably due to the relatively high silver content which would result in a much softer coating. Very little coating wear was measured for coating compositions that had little or no Ag (e.g. see data in Table 2 for coating S-0-0 at room temperature). However, the wear of the counterfaces was more pronounced because the hardness of such coatings was much higher than that of the counterface material. For example, the hardness of the

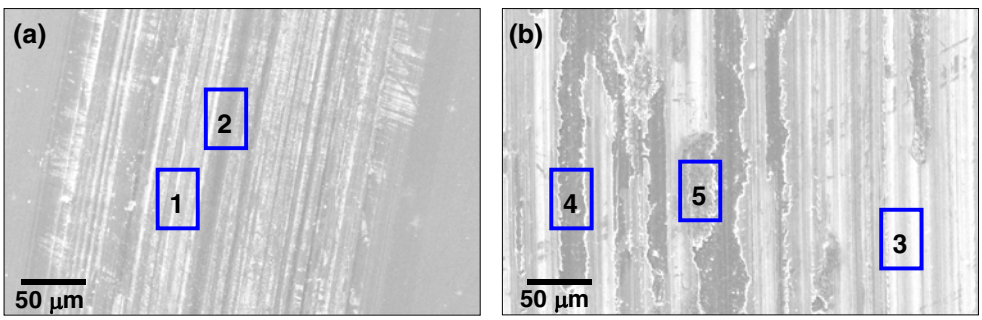

Area 1: Mo(30), N(14), S(11), Ag(14), O(31), Si(0)
Area 2: Mo(22), N(7), S(7), Ag(7), O(56), Si(1)
Area 3: Mo(42), N(13), S(10), Ag(19), O(14), Si(2)
Area 4: Mo(3), N(4), S(0), Ag(1), O(11), Si(3), Fe (78)
Area 5: Mo(19), N(11), S(9), Ag(9), O(35), Si(6), Fe(11)

Fig. 2 SEM micrographs for a S-30-20 coating tested at room temperature (**a**) in dry nitrogen and (**b**) in air against Si_3N_4 balls as counterface materials. Also shown are the elemental compositions (at%) of the different regions identified on the micrographs

Mo_2N coating (S-0-0) was measured to be 30 ± 2 GPa compared to 15, 12, and 5 GPa for Al_2O_3, Si_3N_4, and SS, respectively. Silicon (2–14 at%) was detected by EDX on coating samples tested against Si_3N_4 balls suggesting that ball material transfer to coating wear tracks occurred during testing. The amount of transferred Si increased with decreasing atomic fractions of lubricating phases added to the hard Mo_2N matrix, with the maximum Si detected inside wear tracks for single-phase Mo_2N coating (S-0-0). The addition of MoS_2 and Ag substantially decreased the wear of Si_3N_4 balls, which explains the improved CoF (see Table 2, Si_3N_4/Air). Neither of the Mo_2N/MoS_2/Ag coatings investigated here demonstrated the frictional response of MoS_2, at room temperature. This suggests that the amorphous MoS_2 component in the coating was incapable of developing a surface lubricating film at the contact surface, as observed in previously investigated chameleon coatings [38, 39]. This discrepancy could be the result of the relatively small amount of MoS_2 in the current study.

3.3 350 °C Tests

Table 2 shows the CoF measured at 350 °C for the different Mo_2N/MoS_2/Ag coatings. The results shown in this table indicated that the addition of the lubricious phases provided significant improvements toward reducing friction. For instance, the CoF decreased from $\mu = 0.72$ for pure Mo_2N to 0.37–0.4 for coatings with silver contents in excess of 12 at%, which is typical for hard surfaces lubricated with noble metals in this temperature range [13, 40]. The addition of MoS_2 did not, however, seem to significantly affect the CoF. Shown in Fig. 3 are Raman spectroscopy data for S-27-0 coating outside the wear track

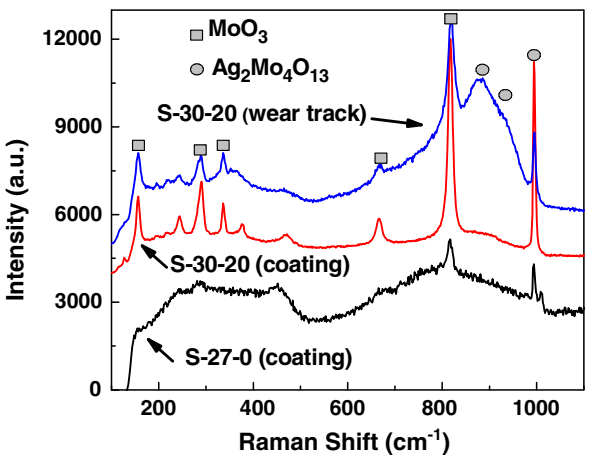

Fig. 3 Raman spectroscopy data for (**a**) S-27-0 coating outside wear track, (**b**) S-30-20 coating outside wear track, and (**c**) S-30-20 coating in wear track, after 350 °C sliding tests against Si_3N_4

(a) and for S-30-20 coating outside (b) and inside (c) the wear track. The Raman data measured for all Mo_2N/MoS_2/Ag coatings revealed that only the α-MoO_3 readily formed on the surface. However, a broad peak in the 850–950 cm^{-1} region was also observed in the wear track, especially for the sulfur-containing coatings, as shown in Fig. 3 for S-30-20. This broad peak could correspond to contributions from the $Ag_2Mo_4O_{13}$ Raman modes with peaks located at 865, 903, and 953 cm^{-1} [19]. Another important phase that formed on the surface of the coatings is pure silver, similar to reports on silver surface diffusion and coalescence at elevated temperatures for other nanocomposite coatings [13, 25, 30]. Silver provides no Raman response and, hence, complementary techniques were used to confirm its presence. XRD and SEM measurements (not shown) indicated that metallic silver formed on the surface of the coatings after heating at 350 °C. Its content in the wear track was found to be higher than in other areas of the coating using both EDX and XPS. Hence, silver and α-MoO_3 are the predominant phases in the wear track. In this temperature range, silver diffusion to the surface is rapid, and controls the sliding mechanism as evidenced by corresponding COF values in Table 2. The formation of α-MoO_3 and very small amounts of $Ag_2Mo_4O_{13}$ in the wear tracks detected with Raman analyses suggest that 350 °C may be close to the onset temperature of chemical reactions in the contact, which reduce friction at higher temperatures and allow for coating self-adaptation to temperature.

3.4 600 °C Tests

Figure 4 shows the friction coefficients for the Mo_2N/MoS_2/Ag nanocomposite coatings at 600 °C. The Mo_2N reference coating (S-0-0) exhibited a high friction coefficient ($\mu = 0.8$) against Si_3N_4 counterfaces. The addition of Ag and/or MoS_2 was found to reduce the friction coefficient substantially. For example, a very low value of $\mu = 0.1$ was obtained for S-30-20 and S-50-40 coatings. This is most significant, since all reported CoF of nitride-based materials against Si_3N_4 had much higher values (in excess of 0.8). Even against alumina counterparts, which typically yield lower friction coefficients, the reported CoF for self-lubricating nitride coatings was significantly higher. For example, Gulbinski and Susko [19] recently reported that the value for Mo_2N/Ag against Al_2O_3 was $\mu = 0.5$ when tested at 400 °C. This was close to that measured in the current work for the Mo_2N/Ag coating (Table 2, coating S-27-0). Also, Kutchej et al. [41] reported CoF values greater than 0.4 for the CrN/Ag system with different Ag contents when tested at 600 °C against Al_2O_3. Unfortunately, neither of these literature reports provide data for tests against Si_3N_4 balls.

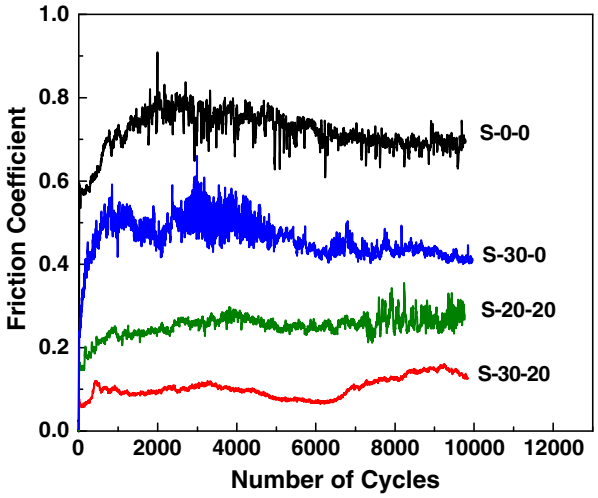

Fig. 4 CoF for selected coatings recorded at 600 °C sliding tests against Si_3N_4

Wear rates were determined by evaluating the topography of the wear tracks using a stylus profilometer. The calculated wear rates, listed in Table 2, clearly demonstrate that the tribological properties of Mo_2N are improved with the addition of lubricious phases. The wear rate for S-50-40 was found to be 8×10^{-6} mm^3/nm, which is approximately two orders of magnitude better than that of Mo_2N (5×10^{-4} mm^3/nm for S-0-0). The wear rate of the balls was also reduced because of the lubricious nature of the coatings.

Figure 5 shows the surface topography of the wear tracks for selected $Mo_2N/MoS_2/Ag$ nanocomposite coatings after 10,000 sliding cycles. The corresponding elemental compositions of different regions in these micrographs were estimated by EDX and were also reported in this figure. Silver was distributed throughout the wear tracks for coatings with silver content greater than 12% (S-20-20, S-30-20, and S-50-40). The bright particles shown outside of the wear track in $Mo_2N/MoS_2/Ag$ coatings correspond to Ag-based agglomerates of various sizes that were uniformly distributed on the coating surface (Fig. 5a). Both the size and density of these particles increased with Ag content in the coatings. The surface topography of coatings with relatively high MoS_2 content is shown in Fig. 5b. Equiaxed grains and one-axis elongated phases appear on the surface of the coatings outside of the wear tracks and some are spread homogeneously in the wear tracks. Similar surface morphology was observed in earlier studies with YSZ-MoS_2−Ag adaptive coatings and was explained by the formation of significant amounts of silver molybdate phases on the surface [25].

To investigate the wear track chemistry and structural changes, phase composition of the surface oxides were evaluated using micro-Raman spectroscopy (Fig. 6). Raman spectroscopy measurements indicated that the surface of the S-0-0 coating consisted primarily of the MoO_2 phase whereas data taken in its wear track revealed the presence of the α-MoO_3 phase in addition to MoO_2. Both phases are the most stable oxides of molybdenum where the oxidation states of Mo are tetravalent and hexavalent for MoO_2 and α-MoO_3, respectively [42]. However, the Raman spectra for $Mo_2N/MoS_2/Ag$ nanocomposite coatings indicated the presence of $Ag_2Mo_4O_{13}$ silver molybdate phase [19] in addition to α-MoO_3 and MoO_2. The formation of the $Ag_2Mo_4O_{13}$ phase rather than the Ag_2MoO_4 or $Ag_2Mo_2O_7$ phases was expected given the relatively large Mo content in the coatings, according to the phase diagram of the MoO_3−Ag_2O system [43]. The Raman spectroscopy data also revealed that coatings with relatively high sulfur content favor the formation of silver molybdate over the formation of molybdenum oxide phases. The formation of silver molybdate compounds was reported to be the result of the reaction $MoS_x \pm Ag \rightarrow AgMoS_x$ with the sulfur atoms being replaced by oxygen atoms at temperatures above 500 °C [25]. This agrees well with reports that sulfur

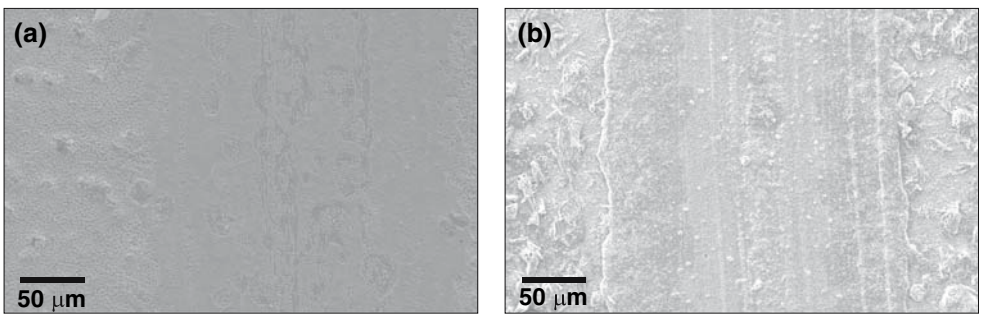

Area 1: Mo(10), N(12), S(1), Ag(36), O(40), Si(1)
Area 2: Mo(9), N(5), S(1), Ag(69), O(9), Si(7)
Area 3: Mo(14), N(15), S(2), Ag(26), O(41), Si(3)
Area 4: Mo(21), N(5), S(3), Ag(7), O(63), Si(1)
Area 5: Mo(13), N(3), S(4), Ag(19), O(60), Si(1)

Fig. 5 SEM micrographs after tribotesting at 600 °C for (**a**) S-30-20 coating and (**b**) S-14-40 coating. Also shown are the elemental compositions (at%) of the different regions identified on the micrographs

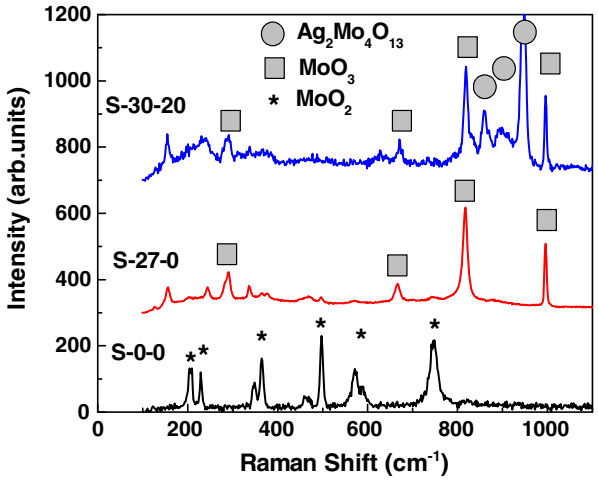

Fig. 6 Raman data from the surface of selected coatings after tribotesting at 600 °C

acts as a catalyst in the formation of lubricious molybdate phases at high temperatures [25]. Thus, $Mo_2N/MoS_2/Ag$ coatings in the current work had maintained a low friction coefficient at high temperatures due to the formation of $Ag_2Mo_4O_{13}$.

Raman spectra were also recorded in different regions of the wear track, as shown in Fig. 7 for S-30-20. Optical micrographs of the regions analyzed with the Raman microprobe are also shown. Under an optical microscope, the majority of the wear track surface is covered by white patches. A much smaller area is covered by black regions where occasional orange spots were seen. Micro-Raman analysis of these regions indicated that: (1) the coating consisted primarily of $Ag_2Mo_4O_{13}$ and α-MoO_3; (2) the white areas in the wear tracks (region 1 in Fig. 7) were exclusively $Ag_2Mo_4O_{13}$, which explains the low measured friction coefficient; (3) the black patches in the wear tracks (region 2 in Fig. 7) were a mixture of $Ag_2Mo_4O_{13}$ and α-MoO_3; and (4) the orange spots in the black areas (region 3 in Fig. 7) corresponded to α-MoO_3. A comparison between Raman data outside and inside the wear track indicates that the contact process between rubbing surfaces promotes the formation of the molybdate phase over the molybdenum oxide phase. This adaptive behavior in friction contact areas was also in agreement with observations made when the coatings were tribotested at 350 °C.

The results of the Raman investigation were confirmed by the XRD data shown in Fig. 8 for S-0-0 and S-30-20 coatings after 600 °C tests. The diffraction peaks for Mo_2N correspond to the tetragonal β-Mo_2N already observed prior to going through the high-temperature wear testing in addition to the monoclinic MoO_2 phase (JCPDS card no.: 78-1,070). In addition to these peaks, the spectra of the $Mo_2N/MoS_2/Ag$ coatings included peaks that matched those of $Ag_2Mo_4O_{13}$, α-MoO_3, and metallic Ag. XPS data were also collected on the coating and in the wear track regions. The main difference between the peak positions measured before and after wear testing was the broadening of the Mo_{3d} peak due to the emergence of peaks reported for the higher valence states Mo^{4+} and Mo^{6+} that correspond to molybdenum oxides MoO_2 (230.0 ± 0.2 eV) and MoO_3 (232.5 ± 0.2 eV), respectively [31]. The other peaks remained at about the same positions (within the accuracy of the measurement) and there was no noticeable difference between the data collected outside and inside wear tracks. Peak intensities, however, changed significantly due to the migration of silver to the surface.

Fig. 7 Raman spectroscopy data for different regions of a S-30-20 coating after tribotesting at 600 °C

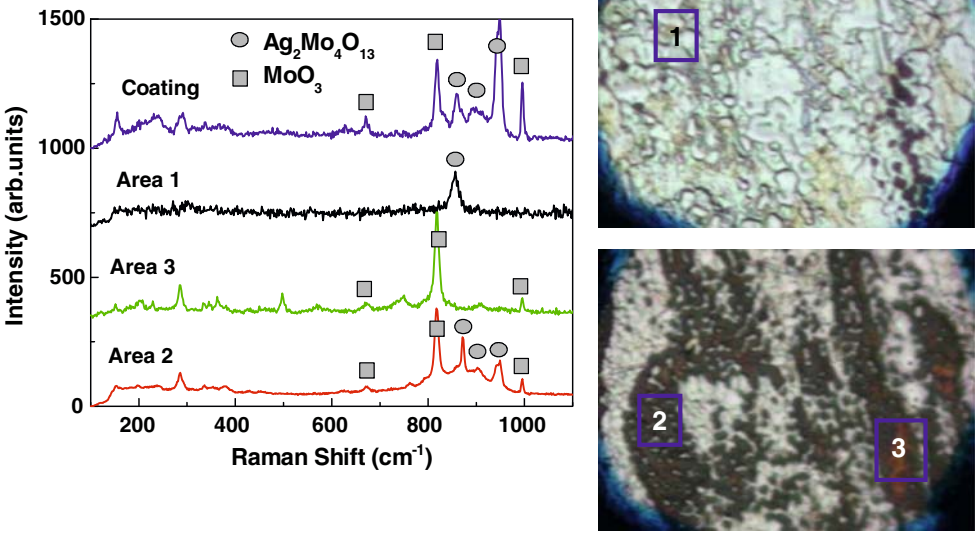

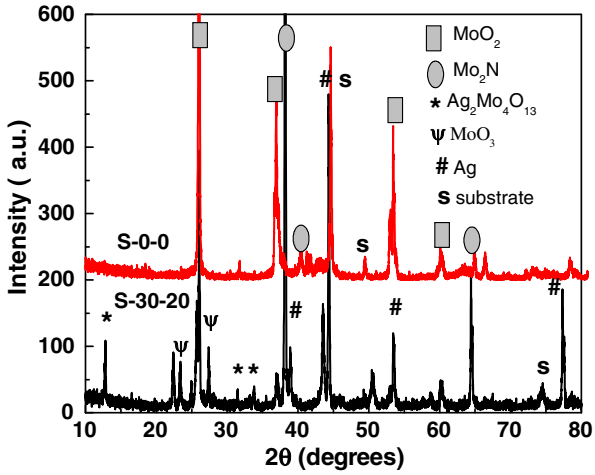

Fig. 8 XRD data for selected coatings after wear testing at 600 °C

4 Conclusions

Composite coatings of $Mo_2N/MoS_2/Ag$ were deposited using unbalanced magnetron sputtering, which included crystalline phases of Mo_2N and silver, and an amorphous MoS_2. The coating composition was systematically varied to provide coatings with β-Mo_2N main phase and additions of MoS_2 and Ag phases, with total variations of 0–13 at% S and 0–24 at% Ag contents. The friction coefficients of these materials were measured at 25, 350, and 600 °C. Relatively high friction coefficients in the range of 0.5–1.0 were recorded when the coatings were tested at room temperature against Al_2O_3, Si_3N_4, and 440C steel counterparts, where tests against Al_2O_3 provided the lowest friction and tests against Si_3N_4 the highest friction coefficients The friction coefficient at room temperature was at the lower range of 0.5 for coatings with a high amount of sulfur; however, the total fraction of amorphous MoS_2 in the coating composition was not significant for providing hexagonal MoS_2 behavior. At higher temperatures, the addition of both Ag and MoS_2 was found to significantly decrease the friction coefficients as a result of the migration of Ag to the surface at 350 °C and the formation of lubricious silver molybdate phases at 600 °C inside wear tracks, which dominated over the formation of molybdenum oxides. The presence of sulfur in the coatings was instrumental in promoting these lubricious phases and achieving temperature-adaptive behavior. The lowest friction coefficient ($\mu = 0.1$) was recorded for samples with Ag content >16 at% and with S content in the 5–14 at% range. This is a significant result given that CoF of self-lubricating nitride-based coatings reported in the literature were significantly higher. The composite $Mo_2N/MoS_2/Ag$ coatings also showed up to a two-order magnitude wear rate reduction in comparison to Mo_2N single-phase coatings. The observed reduced friction coefficients and wear endurance of these composite coatings with a self-lubricating adaptive behavior may be beneficial for friction and wear reduction in hybrid bearings and other mechanical components operating at elevated temperatures.

Acknowledgments This research was supported by the National Science Foundation (award # CMMI-0653986) and by an award from the Air Force Summer Faculty Fellowship Program. The authors also wish to thank Clay Watts of Southern Illinois University and Art Safriet of the Air Force Research Laboratory for their technical assistance.

References

1. Zhong, H.X., Zhang, H.M., Liu, G., Liang, Y.M., Hu, J.W., Yi, B.L.: A novel non-noble electrocatalyst for PEM fuel cell based on molybdenum nitride. Electrochem. Commun. **8**, 707–712 (2006)
2. Shi, C., Zhu, A.M., Yang, X.F., Au, C.T.: On the catalytic nature of VN, Mo_2N, and W_2N nitrides for NO reduction with hydrogen. Appl. Catal. A **276**, 223–230 (2004)
3. Inumaru, K., Baba, K., Yamanaka, S.: Preparation of superconducting molybdenum nitride MoN, ($0.5 \leq x \leq 1$) films with controlled composition. Physica B **383**, 84–85 (2006)
4. Inumaru, K., Baba, K., Yamanaka, S.: Superconducting molybdenum nitride epitaxial thin films deposited on MgO and α-Al_2O_3 substrates by molecular beam epitaxy. Appl. Surf. Sci. **253**, 2863–2869 (2006)
5. Alen, P., Ritala, M., Arstila, K., Keinonen, J., Leskela, M.: Atomic layer deposition of molybdenum nitride thin films for Cu metallizations. J. Electrochem. Soc. **152**, G361–G366 (2005)
6. Lu, J., Kuo, Y., Chatterjee, S., Tewg, J.Y.: Physical and electrical properties of Ta-N, Mo–N, and W-N electrodes on HfO_2 high-k gate dielectric. J. Vac. Sci. Technol. B **24**, 349–357 (2006)
7. Tsui, B.Y., Huang, C.F., Lu, C.H.: Investigation of molybdenum nitride gate on SiO[2] and HfO[2] fro MOSFET application. J. Electrochem. Soc. **153**, G197–G202 (2006)
8. Sarioglu, C., Demirler, U., Kazmanli, M.K., Urgen, M.: Measurement of residual stresses by X-ray diffraction techniques in MoN and Mo_2N coatings deposited by arc PVD on high-speed steel substrate. Surf. Coat. Technol. **190**, 238–243 (2005)
9. Li, X.Y., Tang, B., Pan, J.D., Liu, D.X., Xu, Z.: Tribological properties of Mo–N hard coatings on Ti6Al4V by double glow discharge technique. J. Mat. Sci. Technol. **19**, 291–293 (2003)
10. Woydt, M., Skopp, A., Dorfel, I., Witke, K.: Wear engineering oxides/anti-wear oxides. Wear **218**, 84–95 (1998)
11. Gassner, G., Mayrhofer, P.H., Kutschej, K., Mitterer, C., Kathrein, M.: Magnéli phase formation of PVD Mo–N and W–N coatings. Surf. Coat. Technol. **201**, 3335–3341 (2006)
12. Peterson, M.B., Murray, S.F., Florek, J.J.: Consideration of lubricants for temperatures to 1000°F. ASLE Trans. **2**, 225–234 (1960)
13. Muratore, C., Voevodin, A.A., Hu, J.J., Zabinski, J.S.: Tribology of adaptive nanocomposite yttria-stabilized zirconia coatings containing silver and molybdenum from 25 to 700 °C. Wear **261**, 797–805 (2006)
14. Hauert, R., Patscheider, J.: From alloying to nanocomposites—Improved performance of hard coatings. Adv. Eng. Mat. **2**, 247–259 (2000)
15. Petrov, I., Barna, P.B., Hultman, L., Greene, J.E.: Microstructural evolution during film growth. J. Vac. Sci. Technol. A **21**, S117–S128 (2003)

16. Raveh, A., Zukerman, I., Shneck, R., Avni, R., Fried, I.: Thermal stability of nanostructured superhard coatings: a review. Surf. Coat. Technol. **201**, 6136–6142 (2006)
17. Suszko, T., Gulbinski, W., Jagielski, J.: Mo_2N/Cu thin films—the structure, mechanical and tribological properties. Surf. Coat. Technol. **200**, 6288–6292 (2006)
18. Joseph, M.C., Tsotsos, C., Baker, M.A., Kench, P.J., Rebholz, C., Matthews, A., Leyland, A.: Characterisation and tribological evaluation of nitrogen-containing molybdenum–copper PVD metallic nanocomposite films. Surf. Coat. Technol. **190**, 345–356 (2005)
19. Gulbinski, W., Suszko, T.: Thin films of Mo2N/Ag nanocomposite—the structure, mechanical and tribological properties. Surf. Coat. Technol. **201**, 1469–1474 (2006)
20. Turutoglu, T., Urgen, M., Cakir, A.F., Ozturk, A.: Characterization of Mo2N/Ag nanocomposite coatings produced by magnetron sputtering. Key Eng. Mat. **264–268**, 489–492 (2004)
21. Heo, S.J., Kim, K.H., Kang, M.C., Suh, J.H., Park C.G.: Syntheses and mechanical properties of Mo–Si–N coatings by a hybrid coating system. Surf. Coat. Technol. **201**, 4180–4184 (2006)
22. Liu, Q., Fang, Q.F., Liang, F.J., Wang, J.X., Yang, J.F., Li, C.: Synthesis and properties of nanocomposite MoSiN hard films. Surf. Coat. Technol. **201**, 1894–1898 (2006)
23. Liu, Q., Liu, T., Fang, Q.F., Liang, F.J., Wang, J.X.: Preparation and characterization of nanocrystalline composites Mo–C–N hard films. Thin Solid Films **503**, 79–84 (2006)
24. Voevodin, A.A., Zabinski, J.S.: Nanocomposite and nanostructured tribological materials for space applications. Composites Sci. Technol. **65**, 741–748 (2005)
25. Muratore, C., Voevodin, A.A.: Molybdenum disulfide as a lubricant and catalyst in adaptive nanocomposite coatings. Surf. Coat. Technol. **201**, 4125–4130 (2006)
26. Voevodin, A.A., Zabinski, J.S.: Supertough wear-resistant coatings with 'chameleon' surface adaptation. Thin Solid Films **370**, 223–231 (2000)
27. Erdemir, A.: A crystal chemical approach to the formulation of self-lubricating nanocomposite coatings. Surf. Coat. Technol. **200**, 1792–1796 (2005)
28. Bobzin, K., Lugscheider, E., Nickel, R., Bagcivan, N., Kramer, A.: Wear behavior of $Cr_{1-x}Al_xN$ PVD-coatings in dry running conditions. Wear **263**, 1274–1280 (2007)
29. Mo, J.L., Zhu, M.H., Lei, B., Leng, Y.X., Huang, N.: Comparison of tribological behaviours of AlCrN and TiAlN coatings deposited by physical vapor deposition. Wear **263**, 1423–1429 (2007)
30. Muratore, C., Hu, J.J., Voevodin, A.A.: Adaptive nanocomposite coatings with a titanium nitride diffusion barrier mask for high-temperature tribological applications. Thin Solid Films **515**, 3638–3643 (2007)
31. Badischa, E., Fontalvo, G.A., Stoiber, M., Mitterer, C.: Tribological behavior of PACVD TiN coatings in the temperature range up to 500 °C. Surf. Coat. Technol. **163–164**, 585–590 (2003)
32. Aouadi, S.M., Debessai, M., Filip, P.: Zirconium nitride/silver nanocomposite structures for biomedical applications. J. Vac. Sci. Technol. B **22**, 1134–1140 (2004)
33. Mändl, S., Gerlach, J.W., Rauschenbach, B.: Nitride formation in transition metals during high-fluence high-temperature implantation. Surf. Coat. Technol. **200**, 584–588 (2005)
34. Muratore, C., Voevodin, A.A., Hu, J.J., Jones, J.g., Zabinski, J.S.: Growth and characterization of nanocomposite yttria-stabilized zirconia with Ag and Mo. Surf. Coat. Technol. **200**, 1549–1554 (2005)
35. Kim, G.-T., Park, T.-K., Chung, H., Kim, Y.-T., Kwon, M.-H., Choi, J.-G.: Growth and characterization of chloronitroaniline crystals for optical parametric oscillators I. XPS study of Mo-based compounds. Appl. Surf. Sci. **152**, 35–43 (1999)
36. Wei, Z.B.Z., Grange, P., Delmon, B.: XPS and XRD studies of fresh and sulfided Mo_2N. Appl. Surf. Sci. **135**, 107–114 (1998)
37. Camacho-López, M.A., Escobar-Alarcón, L., Haro-Poniatowski, E.: Haro-Poniatowski, E.: Structural transformations in MoOx thin films grown by pulsed laser deposition. Appl. Phys. A **78**, 59–65 (2004)
38. Wu, J.-H., Rigney, D.A., Falk, M.L., Sanders, J.H., Voevodin, A.A., Zabinski, J.S.: Tribological behavior of WC/DLC/WS2 nanocomposite coatings. Surf Coat Technol **188–189**, 605–611 (2004)
39. Voevodin, A.A., Fitz, T.A., Hu, J.J., Zabinski, J.S.: Nanocomposite tribological coatings with chameleon friction surface adaptation. J. Vac. Sci. Technol. A **20**, 1434–1444 (2002)
40. Erdemir, A., Erck, R.A., Fenske, G.R., Hong, H.: Solid/liquid lubrication of ceramics at elevated temperatures. Wear **203–204**, 588–595 (1997)
41. Kutschej, K., Mitterer, C., Mulligan, C.P., Gall, D.: High-temperature tribological behavior of CrN-Ag self-lubricating coatings. Adv. Eng. Mat. **8**, 1125–1129 (2006)
42. Kumari, L., Ma, Y.-R., Tsai, C.-C., Lin, Y.-W., Wu, S.Y., Cheng, K.-W., Liou, Y.: X-ray diffractiom and Raman scatteringstudies on large-area array and nanobranched structure of 1D MoO_2 nanorods. Nanotechnology **18**, 115717 (2007)
43. Wenda, E.: High temperature reactions in the MoO_3-Ag_2O system. J. Therm. Anal. **53**, 861–870 (1998)